Lasers Med Sci (2016) 31:891–898
DOI 10.1007/s10103-016-1931-x

ORIGINAL ARTICLE

In vitro investigation on Ho:YAG laser-assisted bone ablation underwater

Xianzeng Zhang[1] · Chuanguo Chen[1] · Faner Chen[1] · Zhenlin Zhan[1] · Shusen Xie[1] · Qing Ye[2]

Received: 20 November 2015 / Accepted: 23 March 2016 / Published online: 7 April 2016

Abstract Liquid-assisted hard tissue ablation by infrared lasers has extensive clinical application. However, detailed studies are still needed to explore the underlying mechanism. In the present study, the dynamic process of bubble evolution induced by Ho:YAG laser under water without and with bone tissue at different thickness layer were studied, as well as its effects on hard tissue ablation. The results showed that the Ho:YAG laser was capable of ablating hard bone tissue effectively in underwater conditions. The penetration of Ho:YAG laser can be significantly increased up to about 4 mm with the assistance of bubble. The hydrokinetic forces associated with the bubble not only contributed to reducing the thermal injury to peripheral tissue, but also enhanced the ablation efficiency and improve the ablation crater morphology. The data also presented some clues to optimal selection of irradiation parameters and provided additional knowledge of the bubble-assisted hard tissue ablation mechanism.

Keywords Pulsed Ho:YAG laser · Bone tissue · Laser ablation · Bubble-assisted ablation

Introduction

Surgical lasers have been successfully employed for the ablation of various soft tissue. The potential use of lasers for hard tissue procedures has been paid more and more attention in recent years [1–3]. Compared with conventional mechanical tools such as saws, milling machines and drills, the laser-assisted bone ablation has significant advantages, allowing noncontact intervention, free-cut geometry, and controlled tissue excision with more precision, more comfort, and minimal invasion. Due to the strong absorption of infrared radiation by hydroxyapatite (65 % of the weight of bone) and water (10 to 15 % of the weight of bone) content in bone tissue [4–6], several lasers, including Excimer, Ho;YAG, Er:YAG, Er, Cr:YSGG, CO_2, and FEL, have been investigated for hard tissue ablation and the ablation characteristics dependence on different wavelengths and modes have been reported [7–9]. The primary mechanism for infrared (IR) laser-assisted hard tissue is thermomechanical. Light absorption by water and/or mineral bone components in thin tissue layer can heat interstitial water and lead to internal pressure that reaches the ultimate tensile strength of the tissue, consequently resulting in explosive removal of the outer layers of bone tissue [6, 10].

The temperature elevation during laser-tissue interaction usually leads to thermal damage to surrounding tissue, resulting in carbonization, cracking, and a loss of effectiveness [11, 12]. In order to reduce the thermal injury, an external water spray or water layer on the target tissue surface has been introduced as a cooling agent. Interestingly, the externally supplied water not only reduces the thermal stress but also

Electronic supplementary material The online version of this article (doi:10.1007/s10103-016-1931-x) contains supplementary material, which is available to authorized users.

✉ Xianzeng Zhang
xzzhang@fjnu.edu.cn

✉ Qing Ye
1158113213@qq.com

[1] Institute of Laser and Optoelectronics Technology, Fujian Provincial Key Laboratory for Photonics Technology, Key Laboratory of Optoelectronics Science and Technology for Medicine of Ministry of Education, Fujian Normal University, Fuzhou, Fujian 35007, China

[2] Department of Otolaryngology, Provincial Clinical Medical College, Fujian Medical University, Fuzhou 350004, China

serves to enhance ablation rate and efficiency, improves surface morphology, alters chemical composition, and enhances adhesion to restorative materials [2, 13, 14]. It has been proved that the externally supplied water, rather than water contained in the tissue, significantly influences the effectiveness of the ablation process [28]. Several hypotheses, including bubble formation, hydrokinetic effect, and apatite crystalline fragments, have been proposed to explain the liquid effects on this procedure [15, 16]. However, more detailed studies are needed to reveal the underlying mechanism of liquid-assisted hard tissue ablation.

Previous studies on liquid-assisted hard tissue ablation were conducted mostly with Er:YAG, Er,Cr:YSGG, and CO_2 laser and mainly focused on dental samples. Ho:YAG laser has a relative lower absorption coefficient in water ($\mu_a = 30\ cm^{-1}$), compared to 12480 cm^{-1} at 2.94 μm (Er:YAG), 4180 cm^{-1} at 2.79 μm (Er,Cr:YSGG), and 817 cm^{-1} at 10.6 μm (CO_2) [17]. However, due to its excellent transmission through a flexible fiber, Ho:YAG laser has become a potentially useful tool for arthroscopic and general orthopedic surgeries [18, 19], especially in urology where it has become the preferred lithotripter device [20]. Since Ho:YAG laser is generally performed in a liquid environment, the liquid separating the fiber tip and the tissue surface dramatically absorbs light energy and induces bubble formation, which has important effects on target tissue ablation [21]. However, a detailed study of bubble interaction with hard tissue is not yet clearly discovered; in particular, the dynamic process of bubble-assisted light penetration through a liquid layer and interaction with target tissue, as well as the effects of the related micro-jet kinetic and forces associated with bubble evolution on hard tissue ablation remain unclear. Our previous study [22] showed that the thickness of water layer applied to a tissue surface had significant influences on hard tissue ablation by CO_2 laser. Also, it has been reported [1] that the water layer thickness has important effects on liquid-jet forces associated with the laser-induced bubble. Thus, in the current study, we intend to characterize the bubble induced by Ho:YAG laser, including its formation, expansion, and subsequent collapse, and explore the bubble effects on bone tissue ablation performance in underwater conditions. By applying several thickness of water layer to bone surface, we expect to observe some new features of bubble-assisted bone tissue ablation with Ho:YAG.

Materials and methods

Freshly extracted bovine shank bone used for in vitro laser-tissue ablation experiments were cleaned and saved in normal saline for 24 h. The samples were then cut into rectangular blocks (4 × 1.5 cm with original thickness 5 mm) with a diamond saw. The surface of the bovine shank bone was polished using gritting paper number 800 with a grain size of 30 μm by using a rotary machine. The prepared samples were stored in a saline solution at 4 °C to prevent dehydration. Before the experiment, the bone samples were recovered to room temperature (about 20 °C).

Laser light generated by a free-running pulsed Ho: YAG laser (Wavelight AURIGA, Germany) with a wavelength of 2.08 μm, pulse duration of 350 μs (FWHM), and pulse repetition rate of 3 Hz was transmitted though a low OH^- quartz fiber (NA = 0.22) with a diameter of 600 μm and irradiated on bone sample. The radiant exposure of single pulse was set to a predetermined value 2000 mJ, which was confirmed by reading the laser pulsed energy meter (NOVA II, Orphir, Israel) with a pyroelectric detector. Bone sample was fixed on a customer holder in quartz tank (10 × 10 × 10 cm). In order to evaluate the influence of water layer thickness applied to tissue surface on bubble dynamic and hard tissue ablation, a total of 60 samples were divided into six groups for dry ablation (without water) and liquid-assisted ablation with various water layer thickness (from water surface to fiber tip) ranging from 10 to 30 mm with a step of 5 mm. Free water experiments without tissue sample were conducted as control groups under different water layer thickness. The working distance between the fiber tip and bone surface was fixed at about 1 mm for all bone ablation studies.

Schematic diagram of the experimental setup in the study is shown in Fig. 1. A high-speed camera (PCO.Dimax, Germany) was used for real-time monitoring of the interaction between laser, water, and target tissue. The delay time between the pulse laser and the high-speed camera was controlled by adjusting a digital pulse generator (DG645, Stanford Research System, USA) with overall temporal resolution of 1 ns. A gooseneck fiber optic light guide was used to transport the light from halogen illuminator with the maximum power of 150 W to the diffuser plate as an auxiliary lighting source. A total of ten pulses was applied on each sample location.

The sequential images obtained by a high-speed camera were processed using custom software. Quantitative measurements were performed on the vertical cross-sectional areas of bubble evolving with time, as well as the maximum transversal and longitudinal diameters for each of the different water thickness tested. The morphological changes of the tissue samples were examined by stereomicroscopy (OLYMPUS, SZ61, Japan) with a magnification range extending from ×6.7 through ×45 (using ×10 eyepieces) and a zoom ratio of 6.7:1. The cross-section images of ablation craters were then acquired with an optical coherent tomography (OCT, MOPTIM Co., China) system with lateral and axial resolutions of ~10 μm. The geometries of the cross-section of the crater, including width and depth, were measured based on OCT images using custom software.

Statistical evaluation was performed with a two-tailed t test. A p value of $p \leq 0.05$ indicates a statistically significant effect of the corresponding factor on the measured value. All

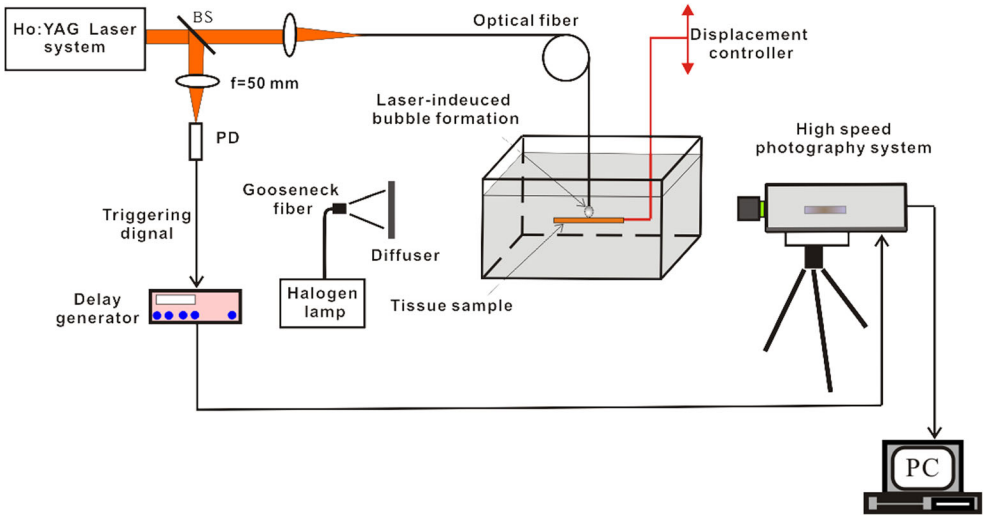

Fig. 1 Schematic diagram of experimental setup for dynamic monitor of bubble and bone tissue ablation induced by Ho:YAG laser

statistical analysis was carried out using SPSS statistical analysis software, version 13.0.

Results

Bubble dynamic

Figure 2 shows the representative images of an evolving bubble induced by Ho:YAG laser under free water with a thickness of 10 mm. The interval between images was about 58 μs. These images showed a whole dynamic process of a bubble induced by laser pulse from its formation to expansion to contraction and subsequent collapse. More than four pulsation periods of bubble were observed with oscillating process including expansion, contraction and collapse. The bubble presented an ellipsoidal shape in the first expansion phase, and then progressively becoming more irregular in shape with increasing time. It is interesting that the bubble departed from the fiber tip at the end of the primary period for all water thickness conditions. The dynamic process of bubble evolution is included in the supplemental information (Supplemental Movies 1).

Figure 3a presents the average vertical cross-sectional areas of bubbles evolving as a function of time and under different water layer thickness ($n = 10$). The images show that the bubble cross-sectional area experiences a similar oscillating process for all water layer thickness observed. The cross-sectional areas and pulsation periods in the primary phase were significantly larger than the following secondary and tertiary phase ($p < 0.05$). For example, under water layer thickness of 10 mm, the maximum cross-sectional area and the pulsation period in the primary duration were about 37 mm^2 and 760 μs, respectively, corresponding to about 13 mm^2 and 360 μs in the secondary duration, and 4 mm^2 and 180 μs in the tertiary duration. Similar features were found in other water thickness conditions as seen in Fig. 3a. The maximum cross-section area and pulsation period in each oscillating duration decreased slightly with increasing water layer thickness, but no significant differences were found ($p > 0.05$). It should be noted that the laser pulse used in the study was 350 μs, less than the bubble expansion time in the primary duration (386 μs for a 10-mm water thickness condition), which suggests that all laser energy was absorbed by water during the first pulsation period. The energy decreased dramatically due to the first bubble collapse and heat transfer effects, resulting in a gradual decrease in the bubble size and duration of the following secondary and tertiary phase.

The maximum transverse width and longitudinal length of the bubble in the primary duration were measured as a function of water depth as showed in Fig. 3b. The error bars indicated the standard deviation. The average longitudinal length for all water conditions were about 8 mm with an average transverse width of about 7 mm. No significant difference was found for different water layer thickness ($p > 0.05$).

Bone ablation underwater

Figure 4 shows representative images of bone tissue ablation induced by Ho:YAG laser under water with thickness of 15 mm. The dynamic process of interaction between laser, water and bone tissue can be followed using the sequential images. The water near the fiber tip absorbed the pulse energy dramatically causing rapid bubble formation and expansion (Fig. 4a). At about 80 μs, the bubble was large enough to touch the tissue surface, forming a channel between the fiber tip and tissue surface (Fig. 4b). Through this channel, the following part of pulse energy could be transmitted through the water layer and impacted on the target surface directly. Figure 4c shows a spark induced by laser-tissue interaction at about 336.5 μs. Although the pulse energy was released at about 350 μs, the bubble continued expanding and reached to maximum volume at about 500 μs (Fig. 4d). The bubble contracted quickly (Fig. 4e) and collapsed at about 910.4 μs, which was accompanied by a

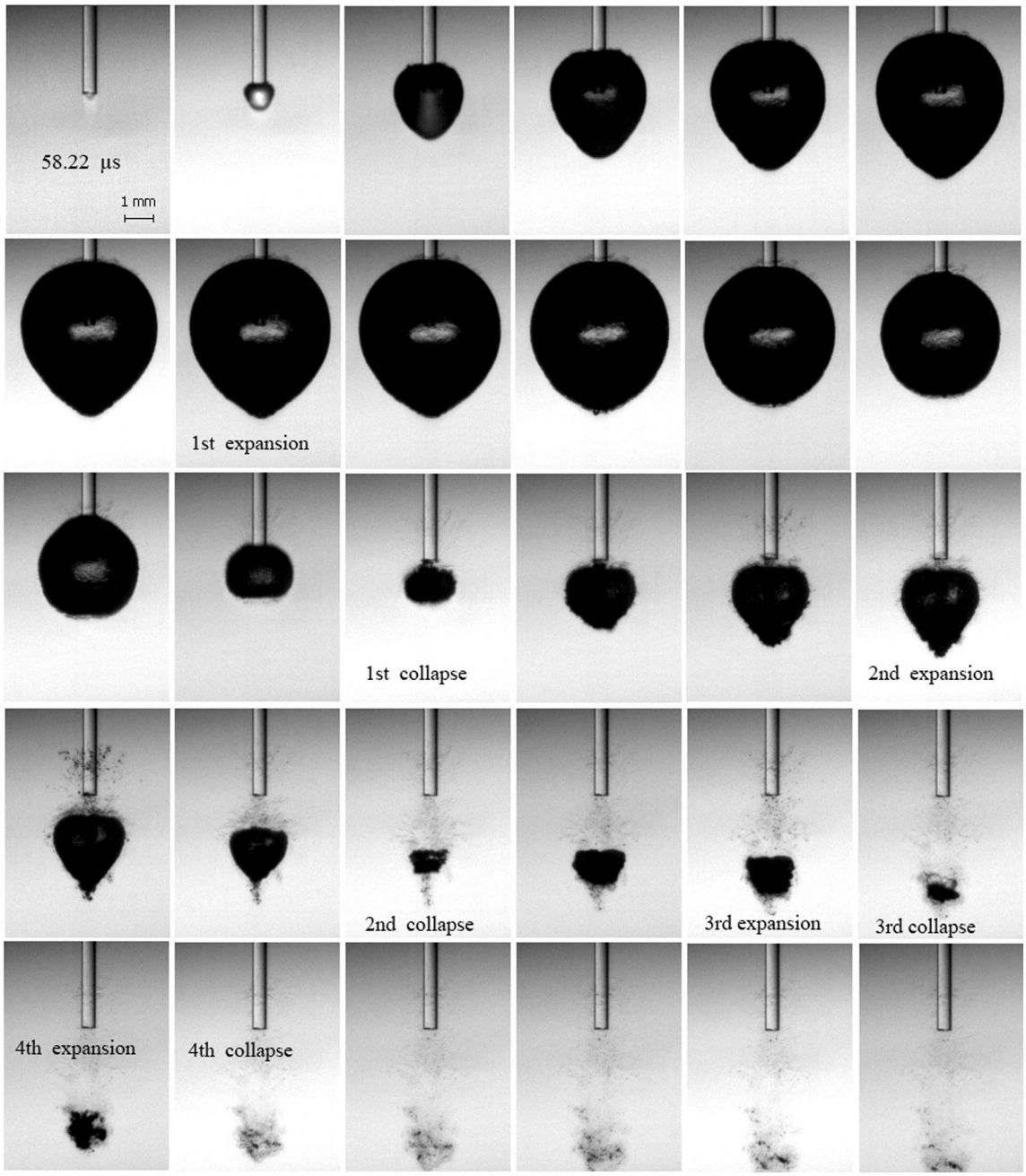

Fig. 2 Representative images of an evolving bubble induced by Ho:YAG laser under free water with a thickness of 10 mm. the interval between images was 58 μs. Scale bar:1 mm

micro-explosion. The ablation debris was ejected into the water during the micro-explosion (Fig. 4f). After that, the bubble experienced several cycles of rebound and collapse (Fig. 4g, h). Each time of bubble collapse was accompanied by a micro-explosion and debris ejection. The liquid movement which carried away ablation debris was seen even after about 2 ms (Fig. 4i). More detailed information about the dynamic interaction of bubble-assisted bone tissue ablation was included in the supplemental information (Supplemental Movies 2).

The top-view stereomicroscope (a–f) and cross-sectional OCT (A–F) images of ablation crater created on bone sample by pulsed Ho: YAG laser in air (dry condition) and underwater with various thickness were shown in Fig. 5, respectively. The ablation crater presented a U-shaped cross-section for all groups of bone samples. Under dry condition, as shown in Fig. 5a, the crater showed irregular surface deformation with a layer of black char formatted and serious thermal damage distributed along the edge of the crater due to excessive heat accumulation during laser irradiation. Whereas, underwater, the ablation craters presented more regular, smooth, and clean features. A whitish area surrounding the ablation crater is observed which may be due to tissue coagulation from thermal

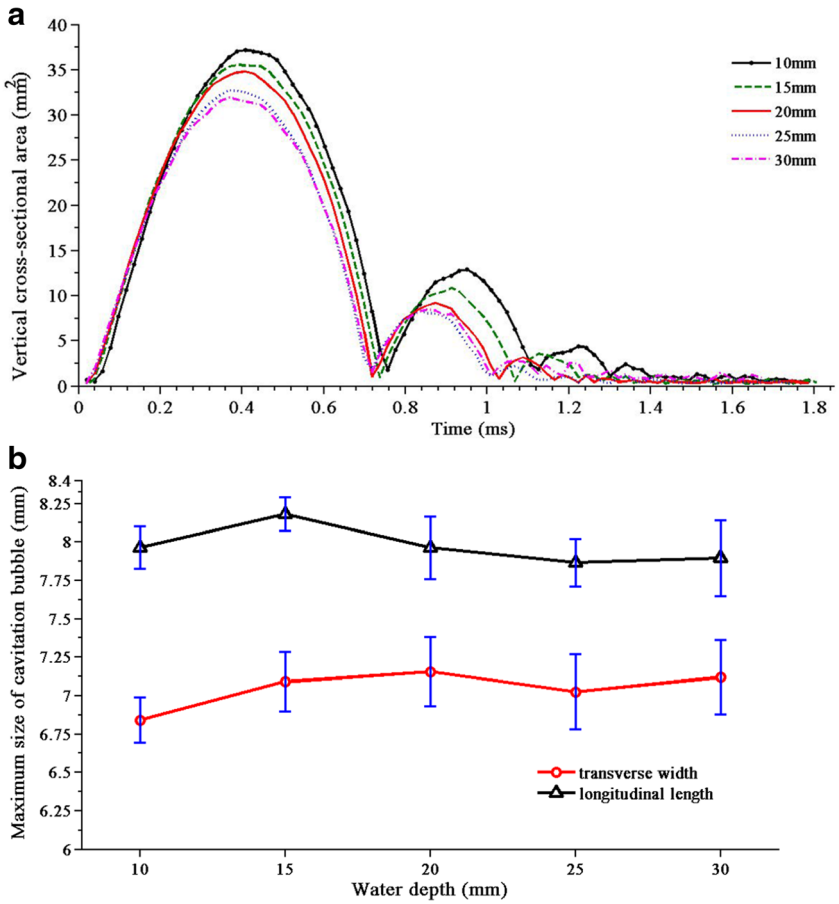

Fig. 3 The average vertical cross-sectional areas of bubble as a function of time (**a**) and maximum size of bubble in primary duration as a function of water layer thickness (**b**). The *error bars* are standard deviation of the data ($n = 10$)

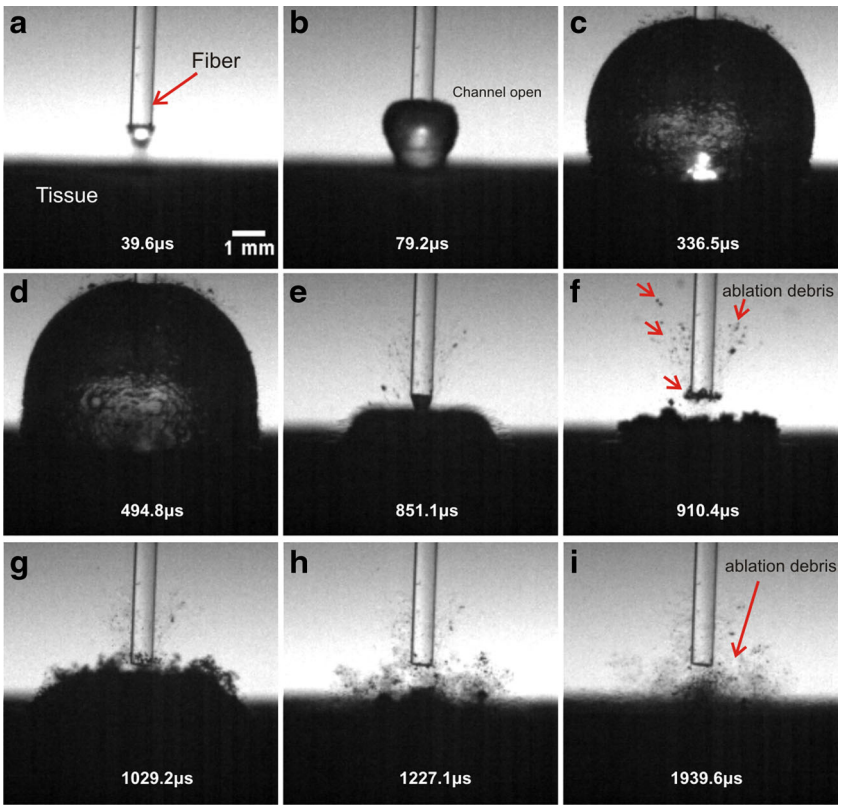

Fig. 4 The representative images of bubble-assisted bone tissue ablation with Ho:YAG laser under water layer thickness of 15 mm. Scale bar: 1 mm

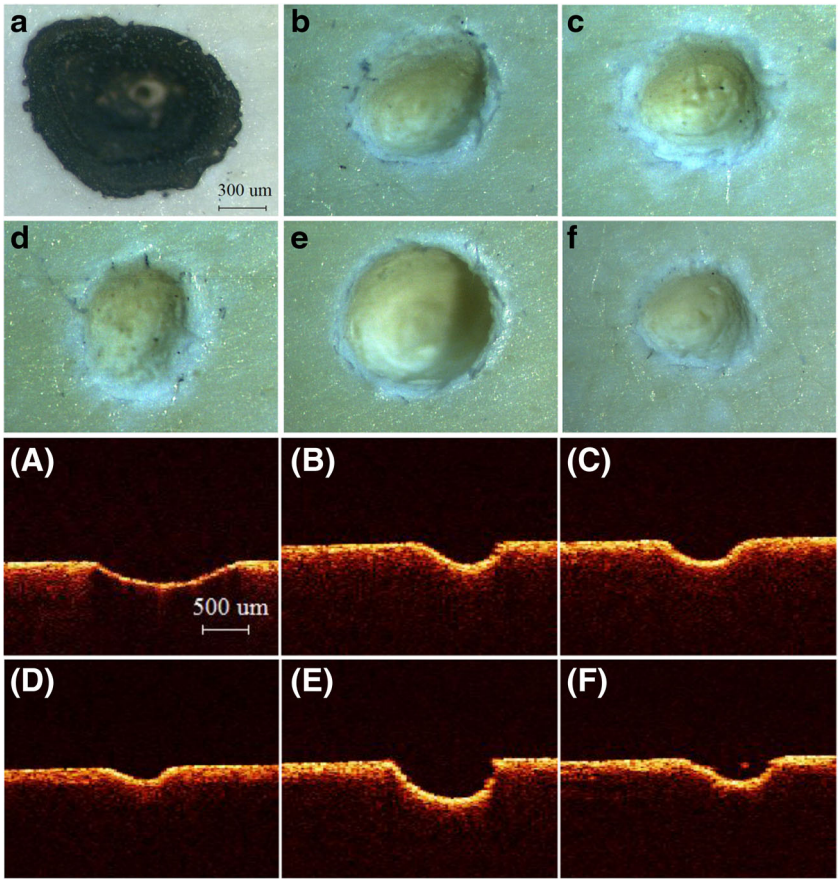

Fig. 5 Top-view stereomicroscope and cross-sectional OCT images of ablation cut created on bone sample by pulsed Ho: YAG laser in air (dry condition) and under water environments. (**a**, A) in air, (**b**–**f**, **B**–**F**) under various thickness of water conditions ranging from 10 to 30 mm with a step of 5 mm, respectively. Pulse number for each crater is 10

damage. No char formation was found under water conditions. It is worth to note that the crater size at a water thickness of 25 mm (Fig. 5e) was larger than the other water conditions tested.

The geometry measurements of the crater created on bovine shank bone as a function of water thickness are shown in Fig. 6. The error bars are the standard deviation of the data. The ablation crater in dry conditions presented a larger size in width yet smaller size in depth than those under water conditions due to thermal injury. It is interesting that the ablation crater width and depth at water layer thickness of 25 mm are larger than the other water conditions ($P < 0.05$).

Discussions

In several clinical application, biological tissue ablation with Ho:YAG laser is generally performed in a liquid environment, for example, in arthroscopic and general orthopedic surgeries, and lithotripsy in urology [18–20]. In the present study, for both free water and bone ablation experiments, the pulsed Ho:YAG laser beam was focused inside the water. As shown in Figs. 2 and 4, the water near the fiber tip absorbed incident laser energy dramatically ($\mu_a = 30\ cm^{-1}$), resulting in the formation of a cavitation bubble. The bubble initially underwent an expansion phase where the pressure and temperature of its

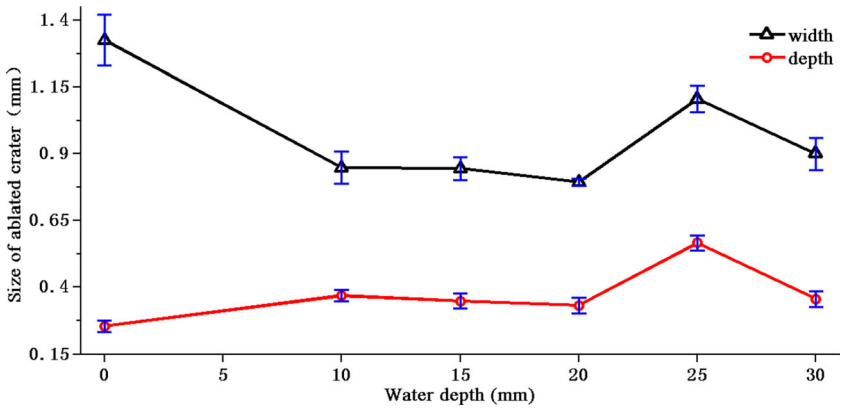

Fig. 6 Ablation size of craters created on the bone sample under different conditions. The *error bars* are standard deviation of the data ($n = 10$)

interior fell and after some time the bubble reached a maximum volume. At this moment, as reported in literature [23] the pressure inside the bubble equals the saturated vapor pressure (about 2330 Pa at 296 K), which is much less than the liquid pressure (about 1 bar). Because of this jump, the bubble starts to contract and is accompanied with a pressure and vapor temperature rise. It is important to note that during contraction, we always have non-equilibrium condensation due to the heat conduction inertia (mainly of vapor). The faster the bubble collapse is, the farther the vapor is from its thermodynamic equilibrium with water. When the vapor pressure and temperature reach their critical values (about 221 bar and 647 K, respectively), the condensation process stops. From this moment, the bubble contracts as if it were filled with "noncondensable vapor," which leads to an even faster rise of the vapor pressure until the contraction stops and the bubble begins to rebound. After experiencing several cycles of expansions and contractions, the bubble finally collapsed. Since gaseous water in the bubble has 100 to 1000 times lower density, this resulted in a much lower absorption coefficient, as compared with liquid water [24, 25]. The bubble formation initiated by the leading part of the pulse energy might contribute to the successive pulse energy transmitted though the water layer and interacted with target tissue (Fig. 4). The average maximum longitudinal length of bubble induced by Ho:YAG laser was up to 8 mm (Fig. 3b), which meant that, with the bubble assistance, the pulse energy penetrated through the water layer up to 4 mm, which is significantly larger than the traditionally held penetration depth of 300 μm [26].

In Fig. 3a, the bubble volume and pulsation period in the primary duration are significantly larger than the following secondary and tertiary phase ($p < 0.05$), which indicates that the deposited energy in the bubble was quickly released during the primary collapse. Figure 4f further showed that the energy released during bubble collapse often occurs with an accompanying micro-explosion. The forces associated with the micro-explosion might impact the ablation crater, causing the ejection and removal of ablation debris (Fig. 4) and result in a smoother and more regular ablation crater than in dry condition (Fig. 5). The channel connecting the fiber to bone surface opened at about 80 μs after laser irradiation and remained opening until about 700 μs. These results suggest how to optimize laser irradiation parameters according to the channel opening time of a bubble to deliver more energy to target tissues through the water layer, thus enhancing ablation efficiency.

Ho:YAG laser at 2.08 μm has been shown to be capable of ablating hard bone tissue effectively under water. As seen in Fig. 5a, irregular surface modification and severe thermal damage (carbonization, charring, and cracking) were associated with dry ablation as a result of excessive heat accumulation. According to Rosa [27], in the black char layer, all the protein and water are removed, and there is significant modification of the mineral phase with loss of carbonate and disproportionation of hydroxyapatite to form other calcium phosphate phases. Unlike in air, the external water layer applied to tissue surface acts as a cooling agent to reduce the thermal damage to periphery tissue around the ablation crater, result in more regular, smoother, and clean incision as compared to the dry condition (Fig. 5). Since the thermal conductivity of water (0.611 W/m·K) is approximately 30 times greater than that of air (0.0267 W/m·K) [7], more thermal can be transferred to the water layer, cooling the target tissue surface via vaporization and convective processes. Moreover, the liquid movement associated with the dynamic process of bubble cycling may also contribute to acceleration of the heat diffusion.

As shown in Fig. 6, although parts of the laser energy were absorbed by water, the ablation depth of the crater under water conditions was larger than those under the dry condition. These features indicated that the water layer applied to the tissue surface actually contributes to enhancing ablation rate and efficiency, as well as fine crater structure, as compared to dry conditions. The forces associated with dynamic bubble movement, especially due to the micro-explosion during bubble collapse, might remove poorly attached nonapatite phases of modified bone. These ablation debris accumulated around the crater might absorb incident light energy dramatically. This process not only induced strong thermal injury to the peripheral tissue (Fig. 5a) but also resulted in a shielding effect and reduced the rate and efficiency of ablation significantly. On one hand, the bubble formation was needed to absorb light energy which might reduce the energy irradiation on tissue sample. On the other hand, however, the forces associated with the bubble dynamic process, especially the micro-explosion generating during bubble collapse (Fig. 4f), might contribute to the removal of ablation debris around the crater, which inversely reduced the energy loss due to absorption by ablation debris and enhanced the ablation efficiency, as well as obtained more regular and smoother ablation crater as compared to air conditions (Fig. 5). It is interesting to note that, as seen in Fig. 6, both ablation width and depth under conditions of 25-mm thickness of water were apparently greater than the other liquid conditions tested ($p < 0.05$). These differences were also observed through stereomicroscope and cross-sectional OCT images (Fig. 5), suggesting that there is a critical thickness of water layer under which the maximum ablation volume could be obtained. The similar critical water layer thickness was reported in our previous study [22]. It has been reported [1] that the liquid-jet force associated with the dynamic bubble process varies with the thickness of water layer and exists a certain water layer thickness where the liquid-jet force has a maximum value. Therefore, the forces and liquid-jet associated with the bubble kinetic process, in particular the micro-explosion during the bubble collapse, might contribute to these features in Fig. 6. However, the detailed mechanisms have not yet been clarified and further studies are needed to explore this phenomenon.

Conclusions

In this work, the complete dynamic process of cavitation bubble induced by a Ho:YAG laser underwater with and without bone tissue, at different water layer thickness conditions, were recorded by high-speed camera. The results showed that, with the assistance of a cavitation bubble, Ho:YAG laser energy could penetrate though the water layer with a thickness up to several millimeters and interact with the target tissue directly. The quick release of energy in the bubble during the collapse process caused a micro-explosion near the tissue surface, which may help to remove the ablation debris, reduce the thermal injury, and improve the morphology of the ablation crater. We also found that the water layer thickness has potential effects on the bubble dynamic process and bone tissue ablation performance.

Acknowledgments This work was partially supported by National Natural Science Foundation of China under Grant No. 61575042 and 61475036 respectively, Natural Science Foundation of Fujian Province (No. 2014J01227), Fujian Provincial department of education Plan Project (JB13022), and the Program for Changjiang Scholars and Innovative Research Team in University (Grant No. IRT_15R10).

References

1. Li B, Wang B, Liu X, He J, Lu J (2015) The jet impact force of laser-induced bubble under the water-film with different thickness. Int Soc Opt Photon. 95430S–95430S
2. Kang HW, Oh J, Welch AJ (2008) Investigations on laser hard tissue ablation under various environments. Phys Med Biol 53(12):3381
3. Stanislawki M, Meister J, Mitra T, Ivanenko MM, Zanger K, Hering P (2001) Hard tissue ablation with a free running Er: YAG and a Q-switched CO2 laser: a comparative study. Appl Phys B 72(1):115–120
4. Izatt JA, Albagli D, Britton M, Jubas JM, Itzkan I, Feld MS (1991) Wavelength dependence of pulsed laser ablation of calcified tissue. Lasers Surg Med 11(3):238–249
5. Youn JI, Sweet P, Peavy GM, Venugopalan V (2006) Mid-IR laser ablation of articular and fibro-cartilage: a wavelength dependence study of thermal injury and crater morphology. Lasers Surg Med 38(3):218–228
6. Forrer M, Frenz M, Romano V, Altermatt HJ, Weber HP, Silenok A, Istomyn M, Konov VI (1993) Bone-ablation mechanism using CO2 lasers of different pulse duration and wavelength. Appl Phys B 56(2):104–112
7. Kang HW, Lee H, Chen S, Welch AJ (2006) Enhancement of bovine bone ablation assisted by a transparent liquid layer on a target surface. Quant Electron IEEE J 42(7):633–642
8. Mirdan BM, Batani D, Volpe L, Villa AM, Bussoli M, Jafer R, Veltcheva M, Procacci P, Conte V (2013) Dental hard tissue ablation using picoseconds pulsed laser emitting at 532 and 266 nm wavelength. J Laser Micro Nanoeng 8(3):192–200
9. Peavy GM, Reinisch L, Payne JT, Venugopalan V (1999) Comparison of cortical bone ablations by using infrared laser wavelengths 2.9 to 9.2 μm. Lasers Surg Med 25(5):421–434
10. Ivanenko M, Werner M, Afilal S, Klasing M, Hering P (2005) Ablation of hard bone tissue with pulsed CO2 lasers. Med Laser Appl 20(1):13–23
11. Shahabi S, Chiniforush N, Juybanpoor N (2013) Morphological changes of human dentin after erbium-doped yttrium aluminum garnet (Er:YAG) and carbon dioxide (CO_2) laser irradiation and acid-etch technique: an scanning electron microscopic (SEM) evaluation. J Lasers Med Sci 4(1):48–52
12. Ekworapoj P, Sidhu S, McCabe J (2007) Effect of different power parameters of Er, Cr:YSGG laser on human dentine. Lasers Med Sci 22(3):175–182
13. Chen S, Emelianov S (2006) Enhancement of high power pulsed laser ablation and biological hard tissue applications. The University of Texas at Austin, Austin
14. Staninec M, Xie J, Le CQ, Fried D (2003) Influence of an optically thick water layer on the bond-strength of composite resin to dental enamel after IR laser ablation. Lasers Surg Med 33(4):264–269
15. Fried D, Ashouri N, Breunig T, Shori R (2002) Mechanism of water augmentation during IR laser ablation of dental enamel. Lasers Surg Med 31(3):186–193
16. Colucci V, Do Amaral FLB, Pécora JD, Palma-Dibb RG, Corona SAM (2009) Water flow on erbium: yttrium–aluminum–garnet laser irradiation: effects on dental tissues. Lasers Med Sci 24(5):811–818
17. Hale GM, Querry MR (1973) Optical constants of water in the 200-nm to 200-μm wavelength region. Appl Opt 12(3):555–563
18. Koslin MG, Martin JC (1993) The use of the holmium laser for temporomandibular joint arthroscopic surgery. J Oral Maxillofac Surg 51(2):122–123
19. Quinn JH (2012) Use of the 2.1 um Holmium: YAG laser in arthroscopic temporomandibular joint surgery. Arthrosc Laser Surg: Clin Appl 275
20. Gupta PK (2007) Is the holmium: YAG laser the best intracorporeal lithotripter for the ureter? A 3-year retrospective study. J Endourol 21(3):305–309
21. Lü T, Xiao Q, Xia D, Ruan K, Li Z (2010) Cavitation effect of holmium laser pulse applied to ablation of hard tissue underwater. J Biomed Opt 15(4):48002
22. Zhang X, Zhan Z, Liu H, Zhao H, Xie S, Ye Q (2012) Influence of water layer thickness on hard tissue ablation with pulsed CO2 laser. J Biomed Opt 17(3):380031–380038
23. Akhatov I, Lindau O, Topolnikov A, Mettin R, Vakhitova N, Lauterborn W (2001) Collapse and rebound of a laser-induced cavitation bubble. Phys Fluids (1994–present) 13(10):2805–2819
24. Mir M, Gutknecht N, Poprawe R, Vanweersch L, Lampert F (2009) Visualising the procedures in the influence of water on the ablation of dental hard tissue with erbium: yttrium–aluminium–garnet and erbium, chromium: yttrium–scandium–gallium-garnet laser pulses. Lasers Med Sci 24(3):365–374
25. Scammon RJ, Chapyak EJ, Godwin RP, Vogel A (1998) Simulations of shock waves and cavitation bubbles produced in water by picosecond and nanosecond laser pulses. Int Soc Opt Photon
26. Scholle K, Lamrini S, Koopmann P, Fuhrberg P (2010) 2 μm laser sources and their possible applications, frontiers in guided wave optics and optoelectronics. In: Bishnu Pal (ed) ISBN: 978-953-7619-82-4, InTech. doi:10.5772/39538. Available from: http://www.intechopen.com/books/frontiers-in-guided-wave-optics-and-optoelectronics/2-m-laser-sources-and-their-possible-applications)
27. Rosa AD, Sarma AV, Le CQ, Jones RS, Fried D (2004) Peripheral thermal and mechanical damage to dentin with microsecond and sub-microsecond 9. 6 μm, 2. 79 μm, and 0. 355 μm laser pulses. Lasers Surg Med 35(3):214–228
28. Meister J, Franzen R, Forner K, Grebe H, Stanzel S, Lampert F, Apel C (2006) Influence of the water content in dental enamel and dentin on ablation with erbium YAG and erbium YSGG lasers. J Biomed Opt 11(3):34030